

Article

Ternary PEO/PVDF-HFP-Based Polymer Electrolytes for Li-Ion Batteries

Hoang Bao Tran Nguyen *, Ling Ding, Björn Pohle , Toni Schmeida , Hoang Bao An Nguyen and Daria Mikhailova *

Leibniz Institute for Solid State and Materials Research (IFW) Dresden e.V., Helmholtzstraße 20, 01069 Dresden, Germany

* Correspondence: h.b.t.nguyen@ifw-dresden.de (H.B.T.N.); d.mikhailova@ifw-dresden.de (D.M.)

Abstract: The impetus to study and develop polymer electrolytes for metal-ion batteries is due to their enhanced safety compared to flammable organic liquid electrolytes, promising ionic conductivity, and broad electrochemical stability window, making them to viable candidates for battery application. In the current work, we present a simple fabrication procedure and a comprehensive physico-chemical study of various PVDF-HFP-based electrolyte formulations with a sufficient addition of PEO polymer, LiTFSI conducting salt, and EMIMTFSI ionic liquid. The ionic conductivity, activation energy for ionic movement and thickness of the resulting polymer electrolyte show a non-linear dependency on the PVDF-HFP/PEO ratio. The electrolyte composition with a 0.35PEO-0.65PVDF-HFP/1LiTFSI/1EMIMTFSI mass fraction exhibits the highest ionic conductivity among the compositions, revealing 7.7×10^{-5} S cm⁻¹ at 30 °C. Electrochemical tests in half full and full Li-ion batteries with a LiFePO₄ cathode and Li₄Ti₅O₁₂ anode also emphasized this composition as the most promising one, providing an initial capacity in full cells of 120 mAh g⁻¹ and a capacity retention of about 75% after 50 charge/discharge cycles at a 0.1 C current rate. In the PEO/PVDF-HFP polymer blend with EMIMTFSI as a plasticizer, the amount of crystalline parts, which are detrimental to a fast ionic diffusion, is significantly reduced.



Academic Editor: Shaokun Chong

Received: 21 November 2024

Revised: 16 January 2025

Accepted: 21 January 2025

Published: 25 January 2025

Citation: Nguyen, H.B.T.; Ding, L.; Pohle, B.; Schmeida, T.; Nguyen, H.B.A.; Mikhailova, D. Ternary PEO/PVDF-HFP-Based Polymer Electrolytes for Li-Ion Batteries. *Batteries* **2025**, *11*, 45. <https://doi.org/10.3390/batteries11020045>

Copyright: © 2025 by the authors. Licensee MDPI, Basel, Switzerland. This article is an open access article distributed under the terms and conditions of the Creative Commons Attribution (CC BY) license (<https://creativecommons.org/licenses/by/4.0/>).

1. Introduction

Rechargeable batteries are currently in high demand due to their high performance and sustainability, e.g., for use in mobile and portable electronic devices and electric vehicles. Lithium-ion batteries (LIBs) are predominantly used for this purpose. The strong increase in demand for LIBs over the last decades necessitates improvement of electrode materials and electrolyte compositions. The electrolyte should not only be chemically stable over a wide voltage and temperature range, but should also have a high Li⁺ conductivity and good compatibility with the electrode materials [1,2]. Besides the classical liquid electrolytes, which are mostly used at present for commercial batteries, the investigation and commercialisation of solid-state electrolytes, e.g., polymer electrolytes, is a new research field. The non-flammability of polymer electrolyte components, heat control, and thus the reduced risk of explosions represent significant advantages in comparison to liquid electrolytes. Furthermore, LIBs with polymer electrolytes can achieve a lower weight and a higher gravimetric energy density, as no additional separator is needed [1,3].

Lithium-polymer batteries are a special form of LIBs, in which the electrolyte is based on a lithium salt and a polymer or polymer blend. Polymer electrolytes used in LIBs, have to fulfil the following conditions: electrical insulation, high ionic conductivity, high mechanical strength, a wide electrochemical stability window, and good chemical and thermal stability [4–6]. In recent years, numerous polymers, such as polyethylene oxide (PEO) [7–12], polyvinylidene fluoride (PVDF) [13] and its copolymer polyvinylidene fluoride-co hexafluoropropylene (PVDF-HFP) [14–17], polyacrylonitrile (PAN) [18], polymethyl methacrylate (PMMA) [19], polyvinylpyrrolidone (PVP) [20], and polyvinyl chloride (PVC) [21], have been investigated for the development of polymer electrolytes. All of them have their own advantages and disadvantages.

Based on the monomer ethylene oxide, PEO is a semi-crystalline polymer whose crystalline phase corresponds to 80% of the entire structure [22]. PEO is the most widely studied polymer for solid electrolyte applications due to its easy complexation with lithium salts, high dielectric constant, and strong solvating ability. In addition, PEO has a low glass transition temperature, good flexibility, and high mechanical stability [2,23,24]. However, the mostly crystalline nature of PEO is a major disadvantage, resulting in poorer conductivity at room temperature [22]. PVDF-HFP is a copolymer based on a crystalline vinylidene fluoride (-VDF) part and an amorphous hexafluoropropylene (-HFP) structure. The crystalline regions offer high mechanical stability, while the lithium ions in the amorphous phase can diffuse easily [25,26]. Furthermore, with a high dielectric constant ($\epsilon = 8.4$) due to the strong electron-withdrawing -C-F group, PVDF-HFP enables completed dissociation of various lithium salts and, thus, a high concentration of the charge carrier [15,27]. In addition, PVDF-HFP can easily be dissolved in many solvents and has a comparatively low degree of crystallinity of about 29% at room temperature [23].

A combination of both polymers can facilitate their advantages and mitigate their disadvantages. A lot of studies on the blending of PEO and PVDF-HFP have been published over the last few years. Zhang et al. [28] prepared PVDF-HFP-based polymer electrolytes with PEO and SiO₂. Here, SiO₂ was added as an inorganic filler to increase the ionic conductivity and improve the thermal stability of polymer electrolytes. The ionic conductivity reached 1.12×10^{-3} S cm⁻¹, and the Li-cell containing LiFePO₄/gel polymer electrolyte/Li showed a high discharge capacity of 146.3 mAhg⁻¹ at 0.1 C-rate (fully charging the cell in 10 h) after 200 cycles. In the work of Manjunatha et al. [29], the polymer blend matrix PEO/PVDF-HFP with 20 wt% LiTFSI salt demonstrated a lower ionic conductivity of 3.14×10^{-6} S cm⁻¹. To improve the ionic conductivity, this electrolyte system was irradiated with oxygen ions. Another method for enhancement of the ionic conductivity is adding a plasticiser. Prabakaran and Manimuthu [6] investigated polymer electrolytes based on a PEO/PVDF-HFP blend matrix with different lithium salts and propylene carbonate (PC) as the plasticiser. The highest ionic conductivity of 8.20×10^{-4} S cm⁻¹ at 30 °C was found in the PEO (6.25 wt%)/PVDF-HFP (18.75 wt%)/PC (67 wt%)/LiTFSI (8 wt%) composition. However, the studies of both Manjunatha et al. [29] and Prabakaran [6] did not show any application of the polymer electrolyte in Li-ion batteries. During the search for a suitable conducting salt for polymer electrolyte systems, many known candidates were tested. According to the work of Ue et al. [30], lithium bis(trifluoromethanesulfonyl)-imide (LiTFSI) has the lowest mobility but the highest dissociation degree compared to LiAsF₆, LiPF₆, LiClO₄, LiBF₄, and LiTf. Furthermore, Kurzweil and Dietlmeier [31] established the following order of ionic conductivity based on data from the study [30] mentioned above: LiPF₆, LiAsF₆ > LiTFSI, LiClO₄ > LiBF₄ > LiTf. The salts with the highest conductivity are inapplicable for polymer electrolytes, since LiAsF₆ is very toxic [32] and LiPF₆ is extremely water-sensitive, irreversibly decomposing to hydrofluoric acid in presence of water [33–35]. Therefore, we chose LiTFSI as a conducting salt for the polymer electrolyte system. As

a plasticiser to reduce the crystallinity of polymers and thereby to increase the ionic conductivity, 1-Ethyl-3-methylimidazolium bis(trifluoromethanesulfonyl)imide (EMIMTFSI) ionic liquid was selected, which contains the same anion TFSI^- to avoid undesirable interactions in the electrolyte. EMIMTFSI exhibits high thermal stability (decomposition temperature above 400 °C) [36], a wide electrochemical stability window from 1 V to 5.3 V vs. Li^+/Li [37], and comparatively high ionic conductivity [38,39].

Ionic mobility occurs mostly in the amorphous phase of the host polymers. The transport mechanism of Li^+ cations in PEO-based polymer electrolytes has been intensively investigated, while the interaction of Li^+ with PVDF-HFP and the corresponding ionic transport are rarely described in the literature. Depending on the concentration of the lithium salt and type of the anion, different $\text{PEO}_x\text{:Li}^+$ complexes can be formed [9,40]. Here, a Lewis acidic Li^+ cation can be coordinated by five ether oxygen atoms of PEO as Lewis bases, thus reducing the mobility of Li^+ . However, local segmental movement of the polymer chains is still possible, whereby the bonding of Li^+ with the oxygen atoms can be broken and Li^+ migrates to the other side of the same polymer chain (intrachain hopping) or into other polymer chains (interchain hopping) (Figure 1a) [2,41,42].

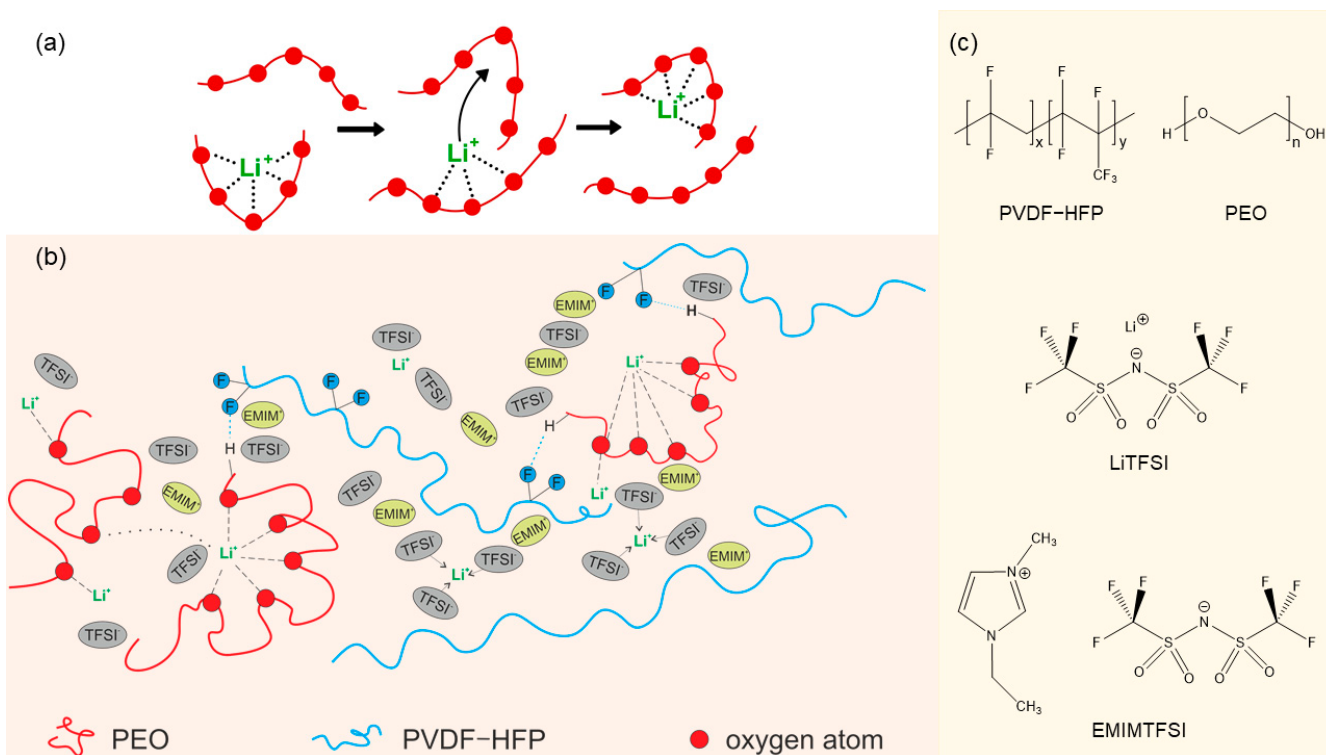


Figure 1. (a) Transport mechanism of lithium cations along PEO chains. The figure was adopted from Meyer [41]. (b) Schematic representation of lithium-ion transport in the ternary PVDF-HFP, PEO, LiTFSI, and EMIMTFSI polymer electrolyte system. (c) Structure of single components PVDF-HFP, PEO, LiTFSI, and EMIMTFSI.

In contrast to PEO, lithium ions are not directly coordinated by the PVDF-HFP polymer chains. On the one hand, due to the chemical inertness of PVDF-HFP, complex formation with lithium cations does not occur. Here, the $-\text{C}-\text{F}$ group in the alkyl chains does not play a role as a Lewis base [3], and the interaction between F-anions and Li^+ is electrostatic in nature and cannot thoroughly compensate for the charge of Li^+ cations. Therefore, some clustering of cations and anions of the salt is possible, since anions are needed for shielding the charge. Here, Li^+ -ions can be at least partially coordinated by anions, which are also present in the ionic liquid. On the other hand, due to the weaker F-Li interaction, this

inactive polymer can support a higher ionic conduction of Li^+ cations. This makes the polymer chains more flexible, which can lead to high segmental movement and subsequent high ionic conductivity [43].

Considering the structures of PEO and PVDF-HFP, an interaction between the two polymer chains can take place. In this case, the hydrogen atoms of PEO can interact with the fluorine atoms of PVDF-HFP, forming intermolecular hydrogen bonds. This results in a more chaotic structure of the polymer blend, which can destroy the crystalline phases and increase the amount of the amorphous phase [26]. Furthermore, ion transport is also affected by the ionic liquid (IL). On the one hand, the electrolyte will be diluted by the addition of IL, resulting in a slight deterioration of the lithium cations' ability to move between the polymer chains. On the other hand, the segmental movement of the polymer chains will be enhanced, improving the overall diffusivity of the lithium ions [44]. Figure 1b shows a possible schematic representation of lithium cation transport in the ternary polymer electrolyte systems under investigation, with all the previously mentioned mechanisms shown together.

In this study, we prepared and characterised a ternary polymer electrolyte (tPE) system containing a PEO/PVDF-HFP polymer blend with LiTFSI and EMIMTFSI. Since the Li^+ coordination and transport mechanisms along both polymers are different, some non-linearity in the properties of the resulting polymer electrolyte is expected. The amounts of lithium salt and ionic liquid in the electrolyte were kept constant, while the mass ratio between PEO and PVDF-HFP was varied as follows: 25 wt%:75 wt%, 30 wt%:70 wt%, 35 wt%:65 wt%, 40 wt%:60 wt%, 45 wt%:55 wt%, and 50 wt%:50 wt%. This corresponds to 1.16 m LiTFSI concentration in the resulting electrolyte formulation. Since two components of the polymer blend have the same molecular weight, the variation in the composition does not affect the total mass of the polymer electrolyte. Various electrolyte compositions were tested in half Li-cells with LiFePO_4 (LFP) and $\text{Li}_4\text{Ti}_5\text{O}_{12}$ (LTO) working electrodes and metallic Li as a counter electrode, and in full cells with a LFP cathode and LTO anode. We clearly observed a positive impact of PEO addition to the polymer blend, which leads, however, to nonmonotoneous changes in properties. This polymer blend system represents a good candidate as a non-toxic, environmentally friendly and easy to fabricate material for applications in lithium-ion batteries.

2. Experimental Section

2.1. Preparation of the Ternary Polymer Electrolytes

The ternary polymer electrolytes were prepared using the casting method (Figure 2). The electrolytes consist of the following components: PEO ($M_w = 400\,000$ g/mol (Sigma Aldrich, St. Louis, MO, USA), PVDF-HFP ($M_w = 400\,000$ g/mol, Sigma Aldrich), conducting salt LiTFSI (>99%, Ossila, UK) and ionic liquid EMIMTFSI (>99%, Ionic Liquid Technologies, Heilbronn, Germany). The mass ratio between polymer, Li-salt and IL corresponded to 1:1:1. Depending on the selected composition, mass proportions of PEO and PVDF-HFP were varied. The prepared and investigated compositions of the ternary polymer electrolytes ($y\text{PEO}/z\text{PVDF-HFP}:\text{LiTFSI:EMITFSI}$ (y, z in wt-%)) are listed in Table 1. Both polymers were dissolved separately in acetone (99%, VWR Chemicals, Darmstadt, Germany), with PEO representing a viscous solution at 40°C , and PVDF-HFP at room temperature. The Li-salt and IL were then added and stirred at 40°C until a homogeneous viscous mixture was obtained.

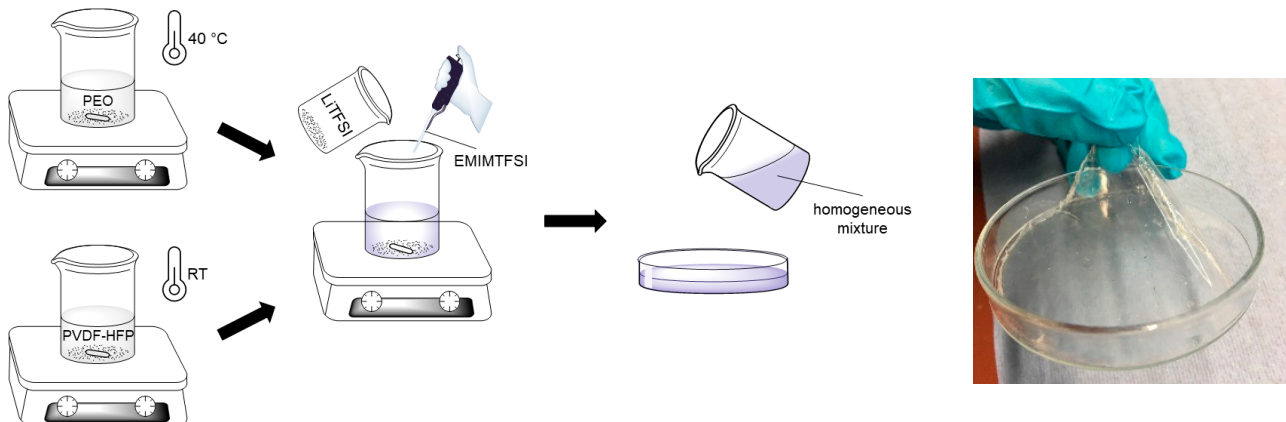


Figure 2. Fabrication scheme of ternary polymer electrolytes using the casting method.

Table 1. Electrolyte compositions and their battery cell designations used in this study. In all compositions, a 1.16 m LiTFSI concentration was realised.

Electrolyte Composition	Name	
25% PEO/75% PVDF-HFP	1 LiTFSI 1 EMITFSI	tPE PEO ₂₅ PVDF-HFP ₇₅
30% PEO/70% PVDF-HFP		tPE PEO ₃₀ PVDF-HFP ₇₀
35% PEO/65% PVDF-HFP		tPE PEO ₃₅ PVDF-HFP ₆₅
40% PEO/60% PVDF-HFP		tPE PEO ₄₀ PVDF-HFP ₆₀
45% PEO/55% PVDF-HFP		tPE PEO ₄₅ PVDF-HFP ₅₅
50% PEO/50% PVDF-HFP		tPE PEO ₅₀ PVDF-HFP ₅₀

2.2. Preparation of the Electrodes

For the electrode mixture, 400 mg active material LiFePO₄ (LFP, Phostech, Elmhurst, IL, USA) or Li₄Ti₅O₁₂ (LTO, >99%, Sigma Aldrich), 50 mg carbon SUPER C65 (TIMCAL, Bodio, Switzerland), and 50 mg binder PVDF (Solvay Speciality Polymers, Alorton, IL, USA) were first mixed and finely ground. The mass ratio corresponded to 80 wt% active material, 10 wt% carbon and 10 wt% PVDF. The finely ground mixture was then suspended for 30 min in a vibration mill from the manufacturer Retsch® (Haan, Germany) at a frequency of 20 Hz with 3 mL of solvent N-methyl-2-pyrrolidone (NMP, 99%, Sigma Aldrich). The suspension was then poured onto an aluminium foil of about DIN A4 size for LFP or a copper foil for LTO. The thickness for the electrodes was set to 200 µm, and a squeegee was used to flatten the suspension and to air-dry it for one day. The next day, the moisture was removed from the coated foils overnight at 80 °C in a drying oven. Before the battery cells were assembled, the electrodes were punched out with a diameter of 12 mm and further dried in the oven in a glovebox for one night at 80 °C.

2.3. Characterisation Techniques

The X-ray diffraction (XRD) measurements were performed using a STADI P diffractometer from STOE in a transmission geometry. The X-ray used corresponded to Cu-K α_1 radiation with a wavelength of 1.54060 Å. The diffractograms were recorded at 2θ angles, which varied from 5° to 90°. The morphology of the ternary polymer electrolytes was analysed using a scanning electron microscope (SEM) (Leo Gemini 1530, Carl Zeiss AG, Oberkochen, Germany) at an acceleration voltage of 5 kV with an SE2 detector. The optical microscopy images were recorded using a digital microscope VHX-7000 from KEYENCE (KEYENCE DEUTSCHLAND GmbH). The Fourier-transform infrared spectroscopy (FTIR) measurements were performed using a Nicolet 6700 (Thermo Fischer Scientific, Dreieich, Germany) in the wavenumber range of 4000–500 cm⁻¹. Thermogravimetry (TG) measure-

ments and differential thermal analysis (DTA) were carried out using a STA 449 C Jupiter device from NETZSCH (Selb, Germany). The measurements were performed in a nitrogen flow with a heating rate of 10 Kmin^{-1} in the temperature range from room temperature to $600\text{ }^{\circ}\text{C}$. The thickness of polymer electrolytes was determined using a digital micrometre. For each polymer electrolyte, the thickness was measured at least four different positions.

2.4. Electrochemical Tests

Galvanostatic cycling with potential limitation (GCPL) tests were carried out using battery coin cells of the CR2025 type (Gelon, China). The cell assembly took place under an argon atmosphere in a glove box, with the H_2O and O_2 content less than 0.1 ppm. Ternary polymer electrolytes were used as a separator. Lithium chips (ChemPUR, Karlsruhe, Germany) with a diameter of 12 mm and a thickness of $250\text{ }\mu\text{m}$ were used as the anode material in half cells. All measurements for the half cells of Li/LFP in a voltage range of $2.0\text{--}4.1\text{ V}$ (vs. Li^+/Li), and Li/LTO $1.0\text{--}3.0\text{ V}$ (vs. Li^+/Li) were performed using a Biologic VMP3 potentiostat in a temperature-controlled climate chamber at $25\text{ }^{\circ}\text{C}$. The full cells of LTO/LFP were tested on a LAND potentiostat from $0.5\text{--}3.0\text{ V}$. Here, the C-rate for all GCPL measurements was 0.1 C. The current required to fully charge or discharge the battery within one hour is defined as 1 C. The mass balancing of both active materials in the full cells was LFP:LTO = $\sim 1:1.2$ (*w/w*), and for all GCPL measurements, and the specific capacities were calculated based on the mass of LFP. Cyclic voltammetry (CV) measurements for determination of the stability window for polymer electrolytes were carried out in different potential ranges, depending on materials, with a scan rate of 0.1 mVs^{-1} . For the potential range from 0 V to 5 V, an asymmetrical cell Al/tPE/Li and a symmetrical cell with stainless steel (SS) were assembled. The asymmetrical SS/tPE/Li cell was measured in the potential range from -2 V to 5 V. The electrochemical impedance spectroscopy (EIS) measurements for calculations of ionic conductivity were performed using an AUTOLAB potentiostat from the manufacturer RHD Instruments (Darmstadt, Germany). The measuring temperature was in the range of $-20\text{ }^{\circ}\text{C}$ to $80\text{ }^{\circ}\text{C}$, with a temperature interval of $10\text{ }^{\circ}\text{C}$. At the end of the experiments, the impedance spectrum was recorded again at $20\text{ }^{\circ}\text{C}$ to control for possible changes in characteristics during measurements. The applied frequencies were varied from 0.1 Hz to 1 MHz and the potential amplitude was 100 mV. To determine the lithium transference number, a symmetrical cell configuration with lithium chips was assembled. Potentiostatic polarisation tests were conducted using chronoamperometry (CA), with an applied voltage of 10 mV for 6 h. EIS was performed before and after the polarisation, utilizing a frequency range of 0.01 Hz to 1 MHz and a potential amplitude of 10 mV.

3. Results and Discussion

3.1. Structure Characterisations

The XRD patterns of pure polymers, their mixture in a 1:1 ratio, fabricated using acetone solution, the conducting salt LiTFSI, mixtures of PEO/LiTFSI/EMIMTFSI (1:1:1), and PVDF-HFP/LiTFSI/EMIMTFSI (1:1:1), and the prepared ternary polymer electrolytes are shown in Figure 3a. Both PEO and PVDF-HFP are semi-crystalline materials in ambient conditions, showing the typical significant crystalline peaks of pure PEO at 19.2° and 23.4° , and of pure PVDF-HFP at 18.4° and 19.9° [24]. The crystalline nature of LiTFSI salt is also confirmed. After mixing of PEO and PVDF-HFP in acetone, followed by evaporation, the crystallinity of PEO is preserved, while reflections of PVDF-HFP drastically decreased, pointing to its pronounced amorphisation. Both the mixtures of PEO/LiTFSI/EMIMTFSI (1:1:1) and PVDF-HFP/LiTFSI/EMIMTFSI (1:1:1), with two broad peaks at 13° and 20° , reflect amorphous behaviour.

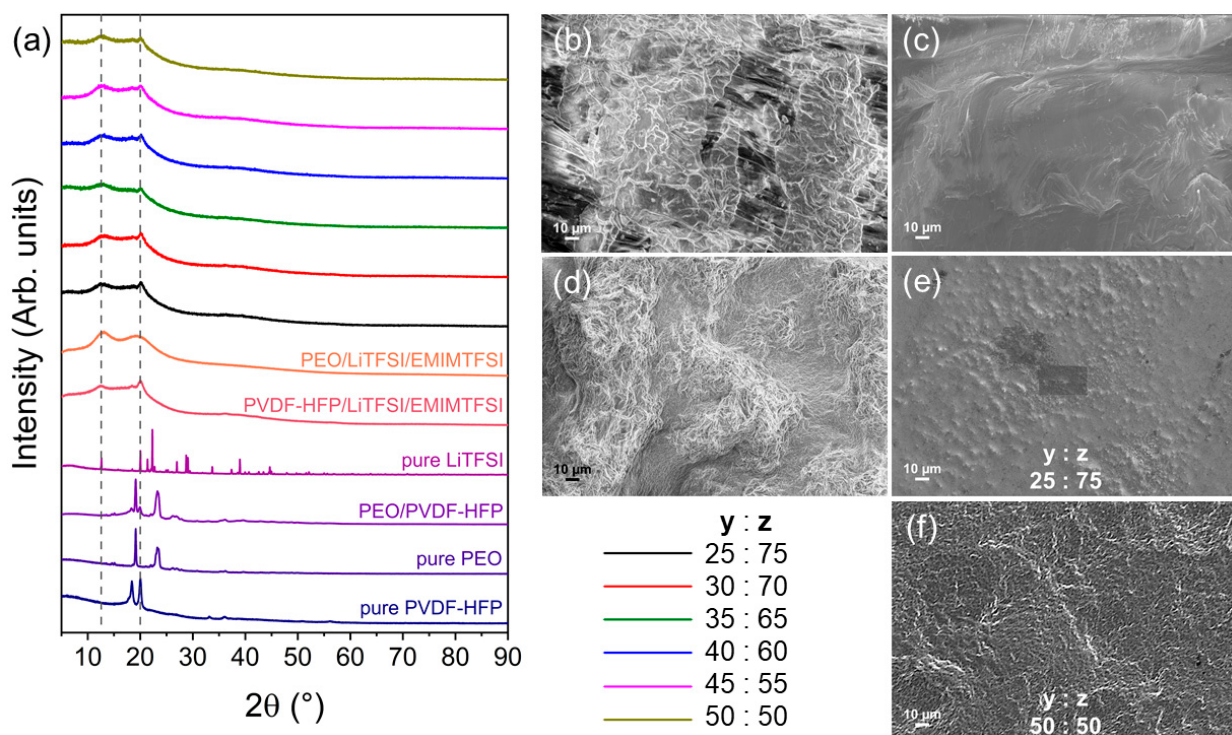


Figure 3. (a) XRD patterns of pure components PVDF-HFP, PEO, LiTFSI, polymer blend PEO/PVDF-HFP (1:1), mixtures of PEO/LiTFSI/EMIMTFSI (1:1:1) and PVDF-HFP/LiTFSI/EMIMTFSI (1:1:1), and ternary polymer electrolytes tPE $\text{PEO}_y\text{PVDF-HFP}_z$, recorded with Cu-K α_1 radiation; (b–f) SEM pictures of: (b) pure PEO, (c) pure PVDF-HFP, (d) polymer blend PEO/PVDF-HFP (1:1), (e) tPE $\text{PEO}_{25}\text{PVDF-HFP}_{75}$, (f) tPE $\text{PEO}_{50}\text{PVDF-HFP}_{50}$.

After ternary electrolyte preparation, the obtained structure is also almost amorphous for all compositions, with two broad peaks at around 13° and 20° . The small crystalline peak at $2\theta = 19.9^{\circ}$, probably of PVDF-HFP, appears in the electrolyte systems, but the intensity is significantly reduced compared to the pure polymer. Moreover, the crystalline peaks of Li salt, observed at about 30° – 50° in the diffraction pattern, and the crystalline peaks of PEO are not visible in the XRD patterns of the polymer electrolytes. This confirms that the composition of both polymers and the addition of the ionic liquid leads to the suppression of the crystallinity.

The surface of the pure polymers, polymer blend (1:1 mass ratio in the polymer matrix), prepared by casting the mixture with acetone and drying at room temperature, and ternary polymer electrolytes were investigated by SEM at 500 times magnification (Figure 3b–f). PEO shows a mosaic/fibre-like structure (Figure 3b), while a smooth structure is observed for PVDF-HFP (Figure 3c). Thus, many polymer fibres appear in the polymer blend matrix due to the presence of a significant amount of PEO (Figure 3d). Accordingly, tPE $\text{PEO}_{25}\text{PVDF-HFP}_{75}$ demonstrates a smoother surface than the surface of tPE $\text{PEO}_{50}\text{PVDF-HFP}_{50}$ due to the high amount of the PEO phase at room temperature. In the presence of LiTFSI and EMIMTFSI, the surface morphology of tPE reflects a more homogeneous structure compared to the PEO/PVDF-HFP polymer blend.

The interactions in the polymer electrolyte can be followed up using FT-IR spectroscopy, with the intensities and shifts of spectral features being interpreted. Figure 4 shows the measured vibrational spectra for all investigated polymer electrolyte compositions: ionic liquid EMIMTFSI, the lithium salt LiTFSI, pure polymers, and the polymer mixture in the wavenumber range of 4000 – 500 cm^{-1} .

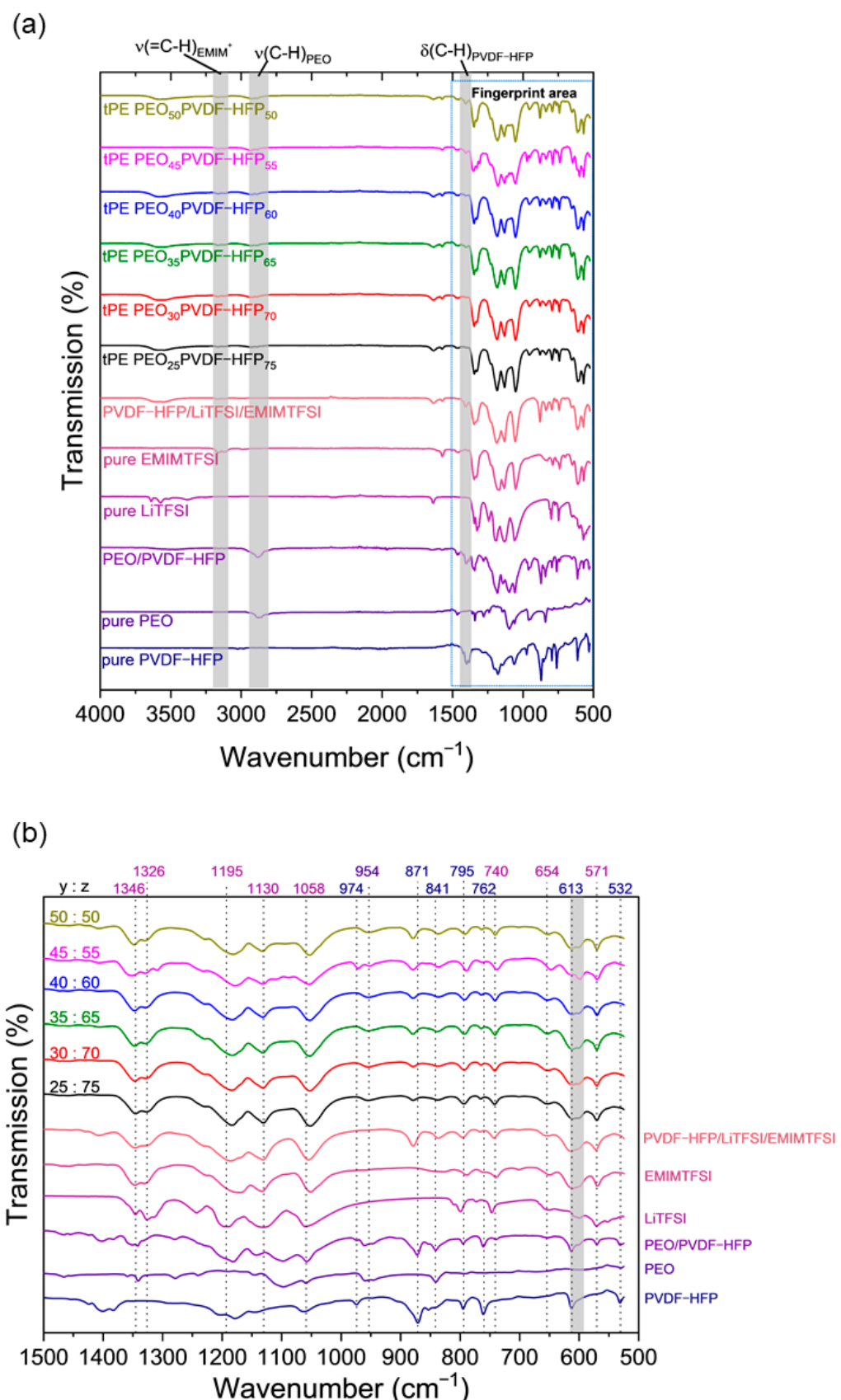


Figure 4. FTIR spectra of tPE PEO_yPVDF-HFP_z, EMIMTFSI, LiTFSI, PEO/PVDF HFP polymer blend with the mass ratio of 1:1, PVDF-HFP/LiTFSI/EMIMTFSI (1:1:1) and individual PEO and PVDF-HFP from 4000–500 cm^{-1} (a), and in the fingerprint region (b).

A pronounced band at 2886 cm^{-1} represents the C-H stretching vibration of PEO [45]. This band appears at 2882 cm^{-1} in the polymer blend and is shifted to $2920, 2922, 2925, 2927, 2933, 2927\text{ cm}^{-1}$ in the ternary polymer electrolyte systems with increasing proportion of PEO. Other significant bands at $1359, 1342,$ and 1100 cm^{-1} define CH_2 wagging, CH_2 bending, and symmetric and asymmetric C-O-C stretching vibration of PEO [29,46]. These bands are not observed in the tPE spectra. The C-O stretching vibration, located at 952 cm^{-1} , shifts to higher wavenumbers (blue shift), while the red shift occurs in CH_2 rocking vibration, located at 841 cm^{-1} .

The slightly visible asymmetric and symmetric stretching vibrations of the C-H bond of PVDF-HFP are subsequently located at 3024 and 2985 cm^{-1} [43], and the deformation vibration is observed at 1400 cm^{-1} [16]. These bands are absent in the tPE spectra. Furthermore, the characteristic vibrational bands of the crystalline phase (α -phase) of PVDF-HFP are assigned at $974, 795, 762, 613$ and 532 cm^{-1} , whereas the bands at 871 cm^{-1} and 841 cm^{-1} identify the amorphous phase (β -phase) of PVDF-HFP. All characteristic bands for the crystalline phase are also absent in ternary polymer electrolyte systems, due to the interactions of all components in the electrolyte and amorphization of crystalline domains.

The bands of the C-H stretching vibration of the imidazolium ring are visible in the range of 3200 – 3100 cm^{-1} [43]. The bands at 1346 cm^{-1} and 1326 cm^{-1} show the asymmetric SO_2 stretching vibration and C-SO₂-N vibration of the LiTFSI and EMIMTFSI. Furthermore, the band at 1193 cm^{-1} represents the symmetric stretching vibration of the CF₃ group of LiTFSI and the C-H vibration of the imidazolium ring of EMIMTFSI, which shift to red in the spectra of the polymer electrolytes. The significant band at 1133 cm^{-1} shows the C-SO₂-N vibration in TFSI[−] anions of LiTFSI and EMITFSI, while the asymmetric S-N-S stretching vibration of the conducting salt and IL is assigned at 1051 cm^{-1} [43]. For more information, other vibration bands are listed in Table S1 in the Supporting Information.

When only PVDF-HFP is mixed with LiTFSI and EMIMTFSI, the resulting spectrum is dominated by features of EMIMTFSI and LiTFSI, with only a tiny contribution of PVDF-HFP. The mixture of PEO with LiTFSI and EMIMTFSI (1:1:1), representing a very viscous and glutinous liquid, was not suitable for measurements.

The IR spectrum of the polymer blend results in a combination of spectra of the individual polymers. The intensities of these bands are either absent or decrease strongly in the presence of the conducting salt and the ionic liquid. This could be explained by possible interactions of the lithium ions and/or the cations of the ionic liquid with the polymer chains taking place. Furthermore, most of the vibrational bands in the spectra of the ternary polymer electrolytes show broadening in comparison to the individual components. It can be assumed that interactions of the Li⁺ and EMIM⁺ cations with the polymer chains also take place. Therefore, the excitation of the vibrations is impeded. A possible explanation for the band shift is the coordination of the PEO chains with the lithium ions and the complexation of the PVDF-HFP chains with the positively charged imidazolium ions. Here, the fluorine atoms, which have the highest electronegativity and a high electron density, are coordinated by the positively charged N-atoms of the imidazolium ring [47]. The complexation could lead to an increase in ionic conductivity. In addition, the crystalline phases of both polymers are suppressed when the ionic liquid is added, which also supports the ionic mobility.

Thermogravimetry and differential thermal analysis were performed to investigate the thermal properties of the ternary polymer electrolytes under consideration. Figure 5 shows the thermal behaviour of the polymer electrolytes in a temperature range from room temperature to $600\text{ }^{\circ}\text{C}$.

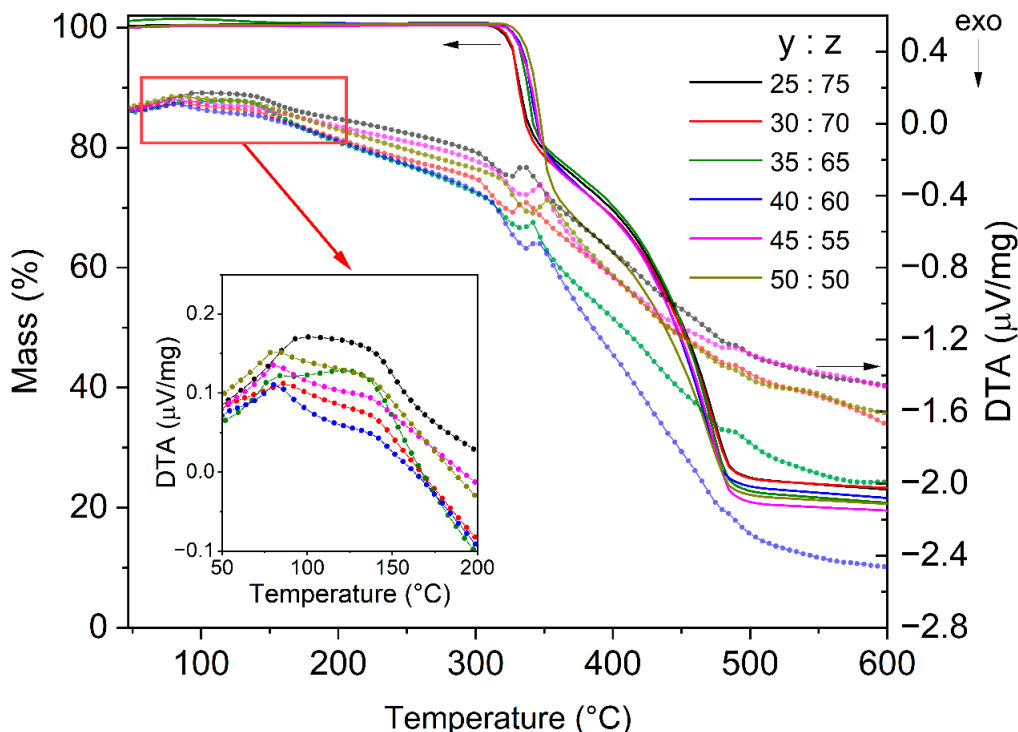


Figure 5. Results of TG/DTA analysis of ternary polymer $\text{PEO}_y/\text{PVDF-HFP}_z/\text{LiTFSI}/\text{EMIMTFSI}$ electrolytes.

In the temperature range below 200 °C, two endothermic signals appear in the DTA curves, the first one at about 77 °C, and the second one at about 137 °C. These two features can be explained by melting of the remaining crystalline domains in both polymers. According to Kurzweil et al. [31], the melting point of PEO is 65 °C and of PVDF-HFP is 135 °C. The small deviation could be explained by interaction of the polymers with other components of the electrolyte systems.

The first mass loss of the ternary polymer electrolytes occurs at around 320 °C, which is visible in the TG curve, followed by the second one at 350 °C. According to Xue et al. [26], structural decomposition of PEO with a mass loss takes place at 194 °C, of PVDF-HFP at 388 °C, and of LiTFSI at 356 °C. EMIMTFSI is thermally stable up to 358 °C [48]. Therefore, the decomposition process results from contributions of all components. The mass loss between 320 °C and 350 °C is about 20% for almost all electrolyte compositions, with the exception of the polymer electrolyte tPE $\text{PEO}_{50}\text{PVDF-HFP}_{50}$, which shows a higher value of 28%. Presumably, this electrolyte is thermally less stable than other compositions due to the large amount of PEO. Decomposition of polymers is accompanied by a strong endothermic signal. This is caused by a combination of the decomposition processes of the CF_3 groups of the PVDF-HFP, ethyl and methyl groups from the imidazolium ring and chain scission of the PEO. The second stage, representing the main decomposition process of the entire structure of the polymer electrolytes, takes place in the temperature range from about 350 °C to 490 °C. Thereby, an endothermic DTA signal is visible here as well.

Although no mass loss can be detected in the TG curve below 200 °C, a change in the polymer structure must have already occurred at this temperature, as the crystalline phases of both polymers have reached their melting points.

3.2. Electrochemical Studies

For a better understanding how interactions between the polymers and other electrolyte components can impact on the performance of batteries, tPE were electrochemically

investigated using electrochemical impedance spectroscopy, cyclic voltammetry, and galvanostatic cycling with potential limitation.

Ionic conductivity. The internal resistance in the tPE systems can be determined using the EIS technique. Figure 6a represents the Nyquist plots of all electrolyte compositions and their resulting circuit model. The component 0.35PEO-0.65PVDF-HFP/1LiTFSI/1EMIMTFSI has the lowest total resistance, in contrast to the electrolyte composition 0.25PEO-0.75PVDF-HFP/1LiTFSI/1EMIMTFSI. In addition, the total resistance changes greatly, according to the temperature change. Figure S1 shows that the Nyquist plot of the component 0.35PEO-0.65PVDF-HFP/1LiTFSI/1EMIMTFSI changed significantly at 20 °C, before and after heating at 80 °C.

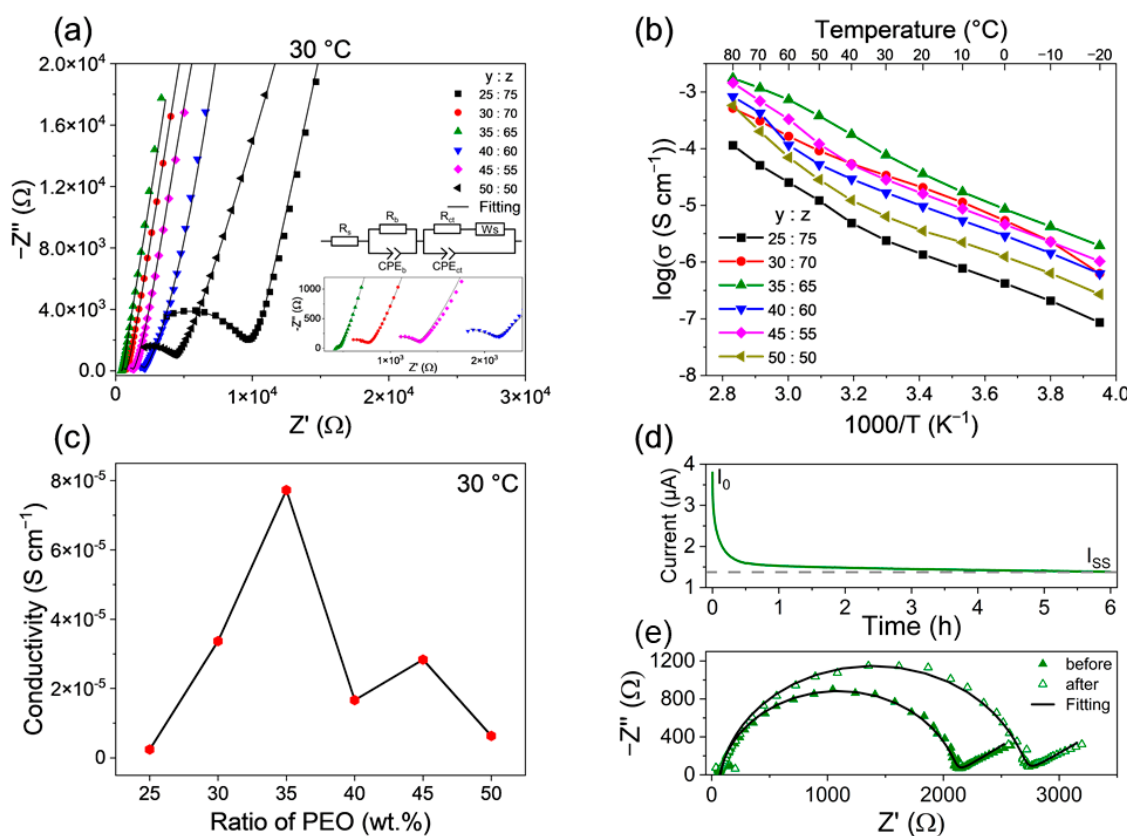


Figure 6. (a) Nyquist plots of polymer electrolytes tPE PEO_yPVDF-HFP_z at 30 °C and the equivalent circuit model with R_s —series resistance, R_b —bulk resistance, R_{ct} —charge-transfer resistance, CPE—constant phase element, W_s —Warburg short element; (b) Ionic conductivity of polymer electrolytes as a logarithmical plot against temperature; (c) Relationship between ionic conductivity and mass ratio of PEO in the ternary electrolyte; (d) Chronoamperogram of tPE PEO₃₅PVDF-HFP₆₅ at 25 °C, and (e) its Nyquist plots before and after polarisation at 25 °C.

The ionic conductivity σ was calculated using the following function from the total resistance, which was determined by the EIS results [26,49].

$$\sigma = \frac{D}{R \cdot A}$$

Here, D is the thickness of the characterised polymer electrolytes, R is the total resistance, and A represents the surface area of the polymer electrolytes. Figure 6b represents the ionic conductivity of polymer electrolytes tPE PEO_yPVDF-HFP_z as a logarithmical plot against temperature. Two distinct regions with different slopes below and above 30 °C can be separated, which still follow Arrhenius-type behaviour. The presence of two ranges can

be explained by a pre-melting process of residual crystalline parts of the electrolyte, which usually occurs far below the melting points of individual polymers and more intensively with a high salt content [50].

Both temperature regions, between $-20\text{ }^{\circ}\text{C}$ and $30\text{ }^{\circ}\text{C}$ and between $30\text{ }^{\circ}\text{C}$ and $80\text{ }^{\circ}\text{C}$, were fitted using the Arrhenius equation, and the activation energy (E_A), which describes the lowest energy required for ion transport in the electric field [26], was calculated for each electrolyte composition.

$$\sigma(T) = \sigma_0 \cdot e^{-\frac{E_A}{kT}}$$

Here, σ_0 is the pre-exponential factor, k is the Boltzmann constant, and T is the temperature in Kelvin.

Table 2 shows ionic conductivity values at $30\text{ }^{\circ}\text{C}$ as well as calculated activation energies for two temperature ranges, between $-20\text{--}30\text{ }^{\circ}\text{C}$ and $30\text{--}80\text{ }^{\circ}\text{C}$.

Table 2. Thickness of ternary polymer electrolytes 1(PEO_yPVDF-HFP_z)-1 LiTFSI-1 EMIMTFSI (y, z in wt%), ionic conductivity and their activation energies in two temperature ranges. For each polymer electrolyte, the thickness was measured at four different points, while the ionic conductivity was determined three times. The values in parentheses represent standard deviations. The activation energy values were calculated using a linear regression model $y = a + b*x$ based on the least squares method; the values in parentheses depict standard deviations.

tPE PEO _y PVDF-HFP _z	Thickness (μm)	Ionic Conductivity at 30 °C (S cm ⁻¹)	E_{A1} (kJ mol ⁻¹) -20–30 °C	R ² Value (E _{a1})	E_{A2} (kJ mol ⁻¹) 30–80 °C	R ² Value (E _{a2})
y	z					
25	75	118(6)	$2.40(8) \times 10^{-6}$	42.2(9)	0.9979	69(2)
30	70	129(3)	$3.40(7) \times 10^{-5}$	50(3)	0.9815	50(2)
35	65	187(2)	$7.7(3) \times 10^{-5}$	47(1)	0.9960	56(3)
40	60	178(6)	$1.70(2) \times 10^{-5}$	41.8(6)	0.9990	72(7)
45	55	182(5)	$2.80(9) \times 10^{-5}$	42.4(2)	0.9999	73(3)
50	50	134(2)	$6.3(3) \times 10^{-6}$	40(1)	0.9961	81(5)

The correlation between the ionic conductivity and the amount of PEO in the polymer electrolyte at $30\text{ }^{\circ}\text{C}$ is shown in Figure 6c. Initially, the ionic conductivity increases with increasing mass proportion of PEO and then tends to decrease. Here, the tPE PEO₃₅PVDF-HFP₆₅ composition reached the highest ionic conductivity of $7.7 \times 10^{-5} \text{ S cm}^{-1}$. This composition may be expected to have the highest specific capacity and cyclic stability. The thickness of the electrolytes also shows a maximum dependence on the composition. The non-linearity in properties must be associated with structure of the electrolyte, including interaction of polymer chains, and its porosity, which should be directly proportional to its thickness, since the total weight of the electrolyte is nearly the same for all compositions. Activation energy for ionic movement in the low temperature range is lower for all electrolyte compositions than in the high temperature range. Apparently, the pre-melting process of crystalline domains in the polymer structure impedes ionic transport.

Lithium-ion transference number. Potentiostatic electrochemical impedance spectroscopy (PEIS) was combined with chronoamperometry to calculate the lithium transference number. This potentiostatic polarisation method was established by Bruce and Vincent for solid binary electrolytes, where the current changes with time in response to applying a small voltage amount ($\Delta V \leq 10 \text{ mV}$) until the cell reaches the steady state and the impedance can be measured before and after potentiostatic polarisation [51]. The transference number t_+ can be calculated by the following equation [52]:

$$t_+ = \frac{I_{SS}(\Delta V - I_0 R_0)}{I_0(\Delta V - I_{SS} R_{SS})}$$

where I_0 and I_{SS} represent the initial and steady state current, which can be interpreted from the chronoamperogram (Figure 6d), ΔV is the applied polarisation voltage of 10 mV, and R_0 and R_{SS} stand for the interfacial resistance before and after polarisation, obtained from the Nyquist plots (Figure 6e), respectively. All determined values and the calculated transference number for three electrolyte systems tPE PEO_yPVDF-HFP_z are shown in Table 3. The Li⁺ transference number slightly decreases with the increase in PEO amount in the ternary polymer film.

Table 3. Determined values and calculated Li⁺ transference numbers of three tPE PEO_yPVDF-HFP_z compositions at 25 °C.

tPE PEO _y PVDF-HFP _z (y:z)	I_0 (μA)	I_{SS} (μA)	R_0 (Ω)	R_{SS} (Ω)	t_+
25:75	5.20	1.69	1437	1816	0.12
35:65	3.80	1.38	2017	2602	0.13
50:50	4.60	1.26	1560	1910	0.10

Electrochemical stability. Figure 7 shows the electrochemical stability window of tPE PEO₃₅PVDF-HFP₆₅ from the cyclic voltammetry between 0–5 V for asymmetrical Al/tPE/Li and symmetrical SS/tPE/SS cell configuration, –2–5 V for asymmetrical SS/tPE/Li cell with a scan rate of 0.1 mV s^{−1}.

For the Al/tPE/Li cell (Figure 7a), a noticeable redox process takes place in the first cycle. This could be caused by the fact that EMIMTFSI is not stable at potentials below 1 V [37]. Starting from the second cycle, the polymer electrolyte system has wide electrochemical stability between 1 V to 5 V. In addition, a Li-Al alloy can form at the potential below 0.5 V. Figure 7b represents the asymmetrical cell configuration with a stainless steel chip at the cathode and lithium chip at the anode. In the first scan, the Li deposition and stripping appear at –0.36 V and 0.22 V. However, some irreversibility and a comparatively smaller peak upon Li stripping are observed due to the redox instability of the EMIM⁺ cations (similar to the case in Figure 7a), which affect the formation process of the solid-electrolyte interface [53]. After the initial cycle, the system exhibits reversibility, but a small peak is observed at 2.4 V, which may be an undesirable reaction between the stainless steel and lithium interface. Figure 7c shows wide electrochemical stability between 0 V and around 4 V in the symmetrical cell configuration with the stainless steel electrodes.

Half cells. The charge-discharge curves for the first cycle and cycle stability are shown in Figure 8a,b for Li/LFP cells, and Figure 8d,e for Li/LTO cells.

In the first cycle, both half cells with LFP and LTO show a relatively high capacity, which is close to the theoretical value (170 mAh g^{−1} for Li/LFP, and 175 mAh g^{−1} for Li/LTO cells). Note that the capacity values in Li/LFP cells do not follow the composition dependence of the ionic conductivity. Thus, the Li/LFP half cells with the lower mass fraction of PEO tend to have a higher specific capacity, except for the tPE PEO₃₅PVDF-HFP₆₅ composition. The cell polarisation, defined as a difference in potentials between the charge and discharge curve at half of the capacity value of the Li/LFP cells, is the lowest for 25% PEO:75% PVDF-HFP, at 165 mV, and increases to 489 mV at higher PEO mass fractions. Considering cycle stability, the discharge capacity of the compositions PEO:PVDF-HFP = 25:75, 35:65, and 50:50 showed around 92% after 50 cycles, compared to the discharge capacity of each composition in the first cycle. Here, the question may arise again of why the long-term performance is not in accordance with the dependence of the ionic conductivity

on the polymer electrolyte composition. While the polymer compositions PEO:PVDF-HFP = 25:75, 30:70, 35:65, and 50:50 showed good stability, the discharge capacities of PEO:PVDF-HFP = 40:60, and 45:55 reduced significantly after 50 cycles. Thus, the discharge capacities were only about 7% and 3.4% of their discharge capacities in the first cycle. A possible explanation for this random relationship and the strongly decreasing capacity could be weak mechanical stability of the LFP electrode–electrolyte interface, leading to contact loss of LFP particles, either to the current collector or to the polymer electrolyte surface due to the volume change in the LFP structure during the lithiation and delithiation. Indeed, LiFePO₄ undergoes a two-phase transformation with the Li-free FePO₄ phase, having a 7% smaller unit cell volume [54]. The interface between the polymer electrolyte and LFP, shown in Figure 7c, features some cracks in the LFP electrode. These areas are definitely less active in the electrochemical process.

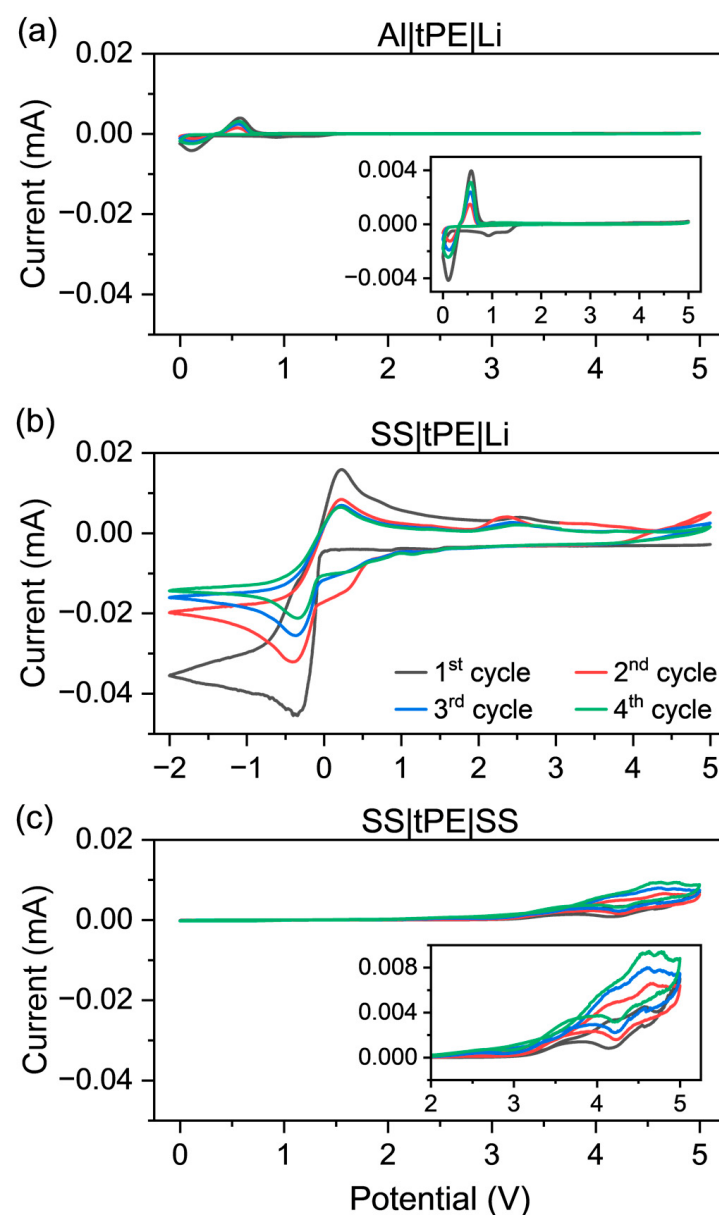


Figure 7. Cyclic voltammograms for tPE PEO₃₅PVDF-HFP₆₅ in asymmetric cell (a) Al|tPE|Li, (b) stainless steel/tPE/Li, and (c) symmetric cell setup with stainless steel at 0.1 mV s⁻¹.

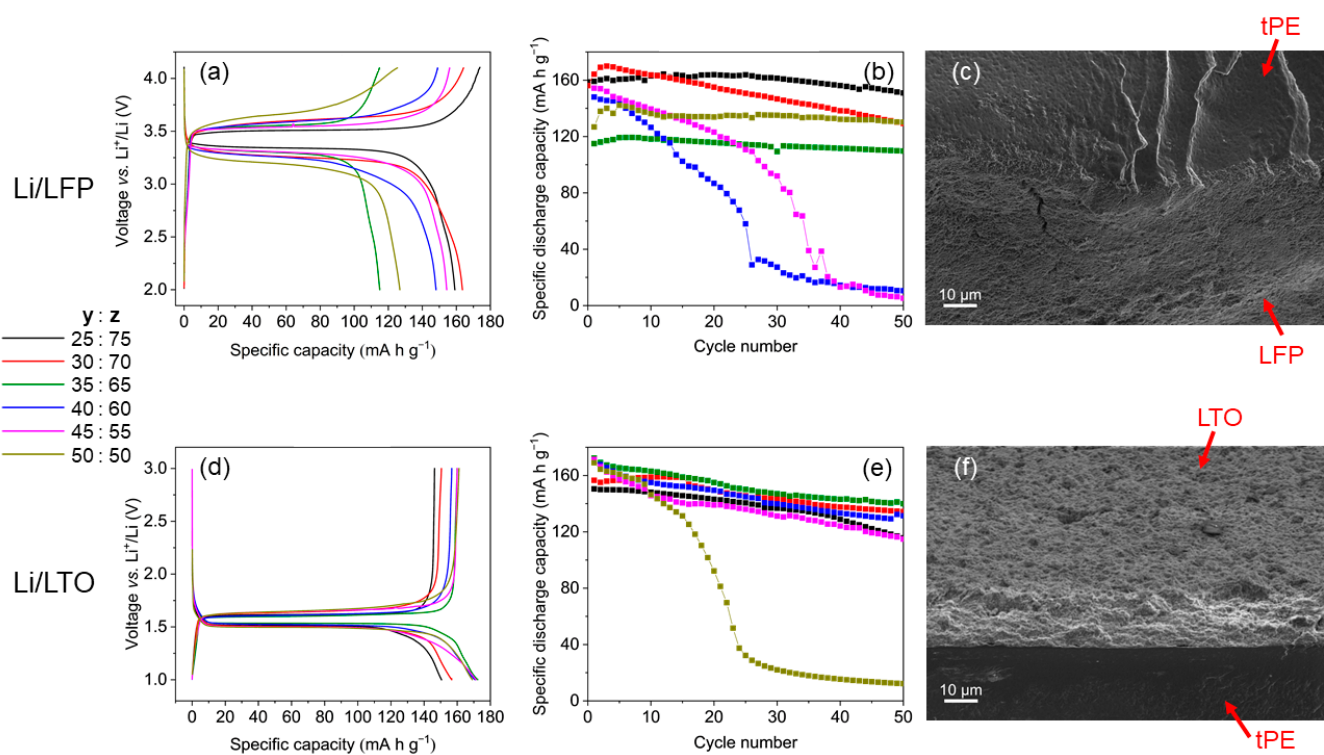


Figure 8. (a) Charge-discharge curve at 25 °C in the 1st cycle (0.1 C) and (b) cycle stability of Li/LFP cells; (c) cutting edge of tPE PEO₃₅PVDF-HFP₆₅/LFP under SEM; (d) charge-discharge curve at 25 °C in the 1st cycle (0.1 C) and (e) cycle stability of Li/LTO cells; (f) cutting edge of tPE PEO₃₅PVDF-HFP₆₅/LTO under SEM; y and z represent the mass ratio (%) of PEO and PVDF-HFP in polymer electrolytes.

The possible corrosion of the lithium salt LiTFSI on the aluminium current collector, reported in the studies [55,56], plays here an inferior role, since it should have the same impact for all compositions.

In contrast to Li/LFP half cells, Li/LTO half cells have a significantly smaller cell polarisation of 73 mV. This increases as the percentage of PEO in the electrolyte system increases, but the difference is less pronounced than for Li/LFP cells. The lowest polarisation of 73 mV occurs in the tPE PEO₃₅PVDF-HFP₆₅ composition, while the highest one of 220 mV belongs to the tPE PEO₅₀PVDF-HFP₅₀ composition, correlating with the ionic conductivity curve vs. composition in Figure 6b. The greater the polarisation, the greater the internal resistance in the electrolyte system. Thus, the internal resistance tends to increase with the increasing weight of PEO. In addition, the Li/LTO half cells represented a very high cycle stability, except for the composition with 50% PEO and 50% PVDF-HFP. The crystallinity of the entire polymer electrolyte system may increase as the crystalline phase of the PEO increases, which can lead to decreasing capacity and stability. In this case, tPE PEO₃₅PVDF-HFP₆₅ showed not only the highest specific discharge capacity, but also the best cycle stability after 50 cycles. Figure 8f depicts SEM images of the layer interface of LTO and the polymer electrolyte. LTO as a “zero-strain” material, demonstrating a very small volume change upon reversible lithiation [57], which is advantageous for interface stability. Rate performance of the tPE PEO₃₅PVDF-HFP₆₅ is shown in Figure 9a. After cycling with different C-rates, from 0.2 C to 2 C, the cell demonstrates high cycle stability at 0.2 C during further 50 cycles.

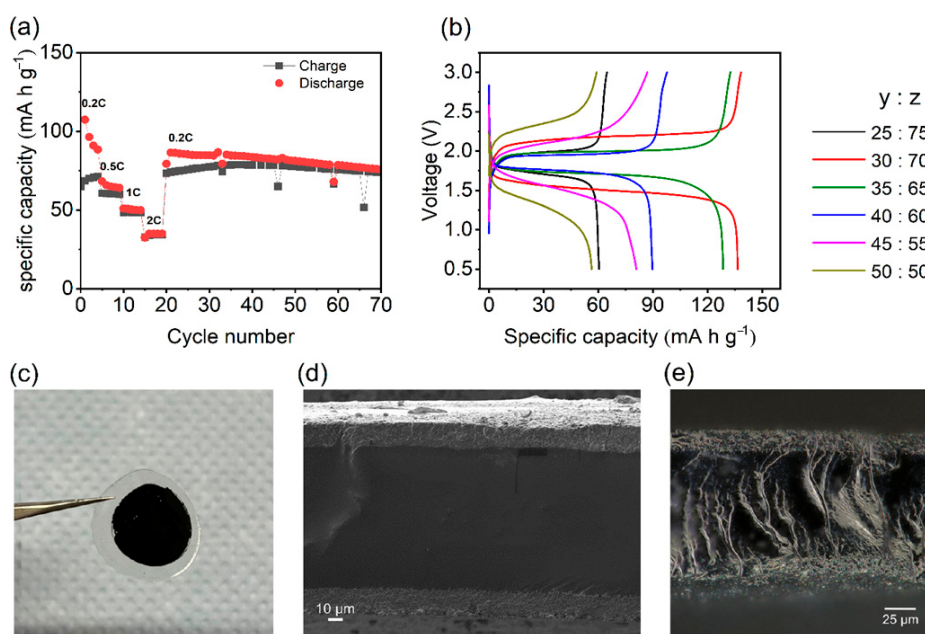


Figure 9. (a) Rate performance of the Li/tPE PEO₃₅PVDF-HFP₆₅/LTO cell; (b) full cells LTO/tPE/LFP in the first cycle; (c) TPE PEO₃₅PVDF-HFP₆₅ with electrode materials after 50 cycles; the sandwich LTO/tPE PEO₃₅PVDF-HFP₆₅/LFP; (d) under SEM and (e) under an optical microscope.

Full cells. Here, Li₄Ti₅O₁₂ served as the anode and LiFePO₄ was the cathode. The mass loadings of both active materials were nearly the same (LFP:LTO = ~1:1.2 *w/w*), and for all GCPL measurements, the results refer to the LFP cathode. One separate formation cycle for the cathode and anode was performed prior to electrochemical tests of full cells.

Figure 9b represents the first cycle of the full cell LTO/LFP with the polymer electrolytes under investigation at 25 °C. The highest specific discharge capacity was 137 mAh g⁻¹, measured for the tPE PEO₃₀PVDF-HFP₇₀ composition. However, this electrolyte composition has a large internal resistance, which can be deduced from the cell polarization of 830 mV. The second-best specific discharge capacity belongs to the polymer electrolyte with a 35% PEO and 65% PVDF-HFP mass ratio. This composition achieved a discharge capacity of 129 mAh g⁻¹, and the corresponding cell polarisation was 640 mV. The electrolyte compositions at y:z = 40:60 and 45:55 reached only about half of the theoretical value. The polymer electrolytes with tPE PEO₂₅PVDF-HFP₇₅ and tPE PEO₅₀PVDF-HFP₅₀ compositions achieved similar specific capacities of only around 60 mAh g⁻¹. However, there were differences between the electrolytes with 25% PEO and 50% PEO concerning polarisation. Furthermore, it is noticeable that the specific capacities decreased with increasing amounts of PEO. The large addition of PEO increases the crystalline part of the entire electrolyte system at room temperature, which limits the ionic transport. To better illustrate how the sandwich of the investigated ternary polymer electrolytes looks after electrochemical measurements, the battery cell with tPE PEO₃₅PVDF-HFP₆₅ after disassembling is shown in Figure 9c. Here, the mechanical integrity of the layers is preserved. This sandwich was also studied under SEM (Figure 9d) and optical microscopy (Figure 9e).

The SEM picture demonstrates a homogeneous structure of the polymer electrolyte in the LTO/tPE PEO₃₅PVDF-HFP₆₅/LFP sandwich, which is significant for high ionic mobility. Under the optical microscope, the polymer fibres are also visible in the electrolyte, which can increase polarisation and facilitate ageing of battery cells.

The cycling stability for 50 cycles is shown in Figure 10. Due to the very low mass ratio of PEO, the tPE PEO₂₅PVDF-HFP₇₅ achieved a lower performance, but the mechanical stability as well as cycle stability were very high, due to the support of the PVDF-HFP chains.

The electrolyte tPE PEO₃₀PVDF-HFP₇₀ has a higher initial capacity but becomes unstable after 50 cycles. This could be caused by the large internal resistance, including the contact resistance. Another possible explanation would be that the interface between the electrode and polymer electrolyte becomes unstable during long-term cycling. The battery cells with the PEO weight percentage of 35% and 40% show a more stable cycling. The capacity loss corresponds to 27% for tPE PEO₃₅PVDF-HFP₆₅ and 48% for tPE PEO₄₀PVDF-HFP₆₀. The full cells with a higher PEO mass fraction of 45% and 50% revealed a significantly lower stability (see Figure S2 in the Supporting Information). Two facts can play an important role here. First, the mechanical integrity of the interface, especially on the LFP/tPE side, is low. Second, the movement of the lithium ions is inhibited by very strong complexation with the PEO polymer chains, whereby not enough mobile ions can participate in the ion transport. For almost all polymer electrolytes, the Coulombic efficiencies reached about 100% and remained constant.

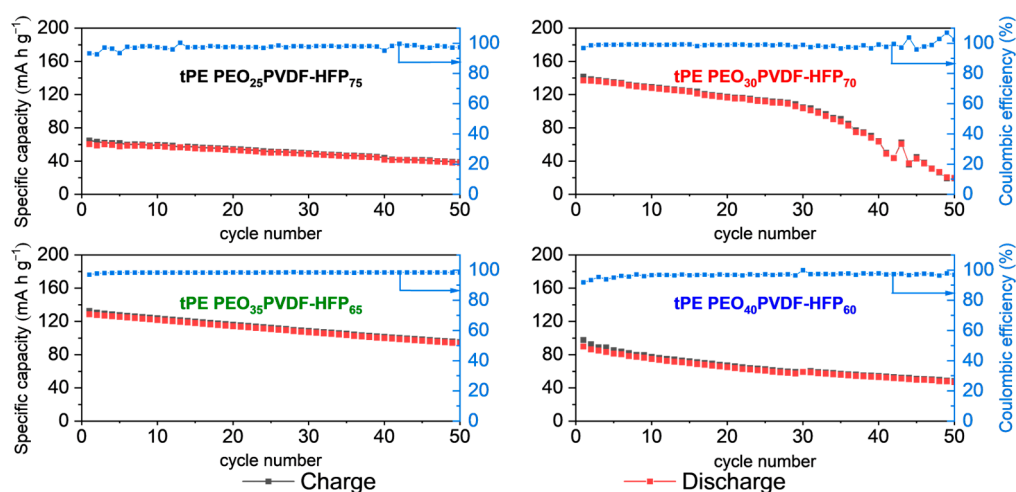


Figure 10. Cycle stability of full cells of LTO/tPE PEO_yPVDF-HFP_z/LFP at 0.1 C at 25 °C.

3.3. Discussion

In lithium-ion batteries with a conventional liquid electrolyte, containing organic solvents and LiPF₆ as a lithium salt, heat generation in the cell occurs, either due to water penetration or a short circuit. Water addition immediately causes dissociation of LiPF₆ with formation of PF₅ and HF. The PF₅ molecules attack solvent molecules, while HF reacts with metallic parts of the battery, producing highly flammable H₂. Altogether, this leads to the combustion of large amounts of active free radicals and thermal runaway of the battery cell [58]. Although PEO is readily flammable, formation of the complex polymer structure with the much less flammable PVDF-HFP and more fire-resistant ionic liquid significantly increases the stability of the whole system. Water addition to the cell system is not expected to be such a detrimental factor, as in case of the liquid LiPF₆-containing electrolytes. However, decreasing the PEO portion in the resulting electrolyte formulation is desirable, despite the promising characteristics of only PEO in a polymer electrolyte composed of 20 wt% PEO/40 wt% LiTDI/40% EMIMTFSI [59].

A nonmonotoneous impact of the PEO amount in the ternary yPEO/zPVDF-HFP:LiTFSI:EMITFSI electrolyte on the electrochemical behaviour in half LFP/Li and LTO-Li cells certainly results from the morphology change of the entire electrolyte film, as well as from a change in the coordination mechanism of Li-cations. The optimal composition corresponds to 35% PEO/65% PVDF-HFP:1 LiTFSI:1 EMITFSI for the operation temperatures of 25° and 60 °C (see Figure S3 in Supplementary Materials). This composition represents a compromise between a facilitated lithium-ion mobility along PEO

polymer chains, and a high amount of detrimental crystalline domains in the overall polymer electrolytes. Moreover, an increased proportion of PEO interrupts the smoothness of the polymer film surface and can also result in weakened mechanical integrity of the interface between the electrode and polymer electrolyte. According to [60], in which room-temperature tensile behaviour of dried PVDF-HFP/PEO membranes with the PEO-composition varied between 0–16% by weight, and wet PVDF-HFP/PEO membranes after absorption of 1M LiBF₄ electrolyte solution of EC and PC (1:1 by weight), was studied, the addition of PEO resulted in significantly lower ultimate tensile strength and modulus in both dried and wet polymer films. The explanation for this was the development of more and larger voids in the sample. The lower stability of the PEO-rich membrane against strain/stress could have a negative impact for the LFP/polymer electrolyte interface during long-term battery cycling. Since the LiFePO₄ cathode material has a noticeable variation in the unit cell volume between the lithiated and lithium-free structure, a weaker mechanical contact at the beginning of cycling becomes worse with time. The cell polarisation, as a difference between the charging and discharging curve at the half of the capacity value, is also enhanced in half and full cells by the electrolytes containing more PEO. We also tested LFP/Li and LTO/Li cells with various electrolyte compositions at 60 °C. At this temperature, close to the melting point of PEO, variation of its amount in the polymer electrolyte should have a higher impact on the electrochemical behaviour of the battery cell. Indeed, the cell polarisation was much higher in case of the LFP/Li cell for all electrolyte compositions in comparison to the LTO/Li cell, which definitely relates to the bigger volume change in the LFP material upon (de)lithiation.

4. Conclusions

In metal-ion batteries, polymer electrolytes based on PVDF-HFP/PEO/EMIMTFSI exhibit less risk for flammability than pure PEO, since PVDF-HFP and EMIMTFSI are much less flammable. Although the estimated costs for the polymer electrolyte film in a battery cell are approximately two times higher than the conventional LP30 electrolyte with a Whatman separator, the increased stability makes polymer electrolytes advantageous for a stationary battery application and scaling up process. We prepared and characterised 1(PEO_yPVDF-HFP_z)-1 LiTFSI-1 EMIMTFSI ternary polymer electrolytes of different compositions ($25 < y < 50$, $75 > z > 50$), which were electrochemically investigated in Li/LFP and Li/LTO half cells as well as in LTO/LFP full cells at 25 °C. The role of the PEO amount for the electrochemical performance was evaluated, and the optimal electrolyte composition was suggested. Despite the somewhat low specific capacity in Li/LFP half cells, the electrolyte formulation containing 35% PEO/65% PVDF-HFP:1 LiTFSI:1 EMITFSI exhibits the highest overall ionic conductivity of 7.7×10^{-5} S cm⁻¹, one of the highest specific capacities and the best long-term stability in LTO/LFP full cells. This composition accumulates a facilitated lithium-ion mobility along PEO polymer chains and a low amount of disruptive crystalline domains in the overall structure of the polymer electrolyte film. To further enhance the electrochemical performance of a full battery cell with the optimal electrolyte composition, mechanical stability of the electrode–electrolyte interface should be increased.

Supplementary Materials: The following supporting information can be downloaded at: <https://www.mdpi.com/article/10.3390/batteries11020045/s1>, SI contains analysis of IR spectra, EIS data, cycling stability results and SEM image for some electrolyte compositions. Figure S1: Nyquist-plots of tPE PEO₃₅PVDF-HFP₆₅ at 20 °C, recorded for materials before and after heating to 80 °C. Figure S2: Left: Cycle stability of full cells LTO/tPE PEO_yPVDF-HFP_z/LFP with a high mass fraction of PEO at 0.1C at 25 °C. Right: SEM image of the sandwich LTO/tPE PEO₅₀PVDF-HFP₅₀/LFP after cycling, reflecting a low mechanical integrity. Figure S3: Charge-discharge curves of half-

cells LFP/tPE PEO_yPVDF-HFP_z/Li (left) and LTO/tPE PEO_yPVDF-HFP_z/Li (right) with various electrolyte compositions at 60 °C. Table S1: Vibrations assigning in IR spectra [16,29,43,45,46,61].

Author Contributions: H.B.T.N.: Conceptualization, Methodology, Investigation, Data curation, Visualization, Writing—original draft. L.D.: Investigation, Validation, Formal Analysis. B.P.: Investigation, Formal analysis, Validation. T.S.: Investigation, Formal analysis. H.B.A.N.: Investigation, Formal analysis. D.M.: Conceptualization, Writing—review and editing, Supervision, Project administration, Funding acquisition. All authors have read and agreed to the published version of the manuscript.

Funding: This work was funded by the German Research Foundation (DFG), project number 462115051.

Data Availability Statement: The original contributions presented in this study are included in the article and Supplementary Materials. Further inquiries can be directed to the corresponding authors.

Acknowledgments: The authors are deeply grateful to Nikolai Gaponik (Dresden University of Technology, Germany) for a fruitful discussion.

Conflicts of Interest: Authors declare no conflicts of interest.

References

1. Goodenough, J.B.; Kim, Y. Challenges for rechargeable Li batteries. *Chem. Mater.* **2010**, *22*, 587–603. [[CrossRef](#)]
2. Xue, Z.; He, D.; Xie, X. Poly(ethylene oxide)-based electrolytes for lithium-ion batteries. *J. Mater. Chem. A Mater.* **2015**, *3*, 19218–19253. [[CrossRef](#)]
3. Osada, I.; de Vries, H.; Scrosati, B.; Passerini, S. Ionic-Liquid-Based Polymer Electrolytes for Battery Applications. *Angew. Chem.* **2016**, *128*, 500–513. [[CrossRef](#)] [[PubMed](#)]
4. Long, L.; Wang, S.; Xiao, M.; Meng, Y. Polymer electrolytes for lithium polymer batteries. *J. Mater. Chem. A Mater.* **2016**, *4*, 10038–10069. [[CrossRef](#)]
5. Costa, C.M.; Nunes-Pereira, J.; Rodrigues, L.C.; Silva, M.M.; Ribelles, J.L.G.; Lanceros-Méndez, S. Novel poly(vinylidene fluoride-trifluoroethylene)/poly(ethylene oxide) blends for battery separators in lithium-ion applications. *Electrochim. Acta* **2013**, *88*, 473–476. [[CrossRef](#)]
6. Prabakaran, P.; Manimuthu, R.P. Enhancement of the electrochemical properties with the effect of alkali metal systems on PEO/PVdF-HFP complex polymer electrolytes. *Ionics* **2016**, *22*, 827–839. [[CrossRef](#)]
7. Croce, F.; Appetecchi, G.B.; Persi, L.; Scrosati, B. Nanocomposite polymer electrolytes for lithium batteries. *Nature* **1998**, *394*, 456–458. [[CrossRef](#)]
8. Christie, A.M.; Lilley, S.J.; Staunton, E.; Andreev, Y.G.; Bruce, P.G. Increasing the conductivity of crystalline polymer electrolytes. *Nature* **2005**, *433*, 50–53. [[CrossRef](#)] [[PubMed](#)]
9. Vallée, A.; Besner, S.; Prud'Homme, J. Comparative study of poly(ethylene oxide) electrolytes made with LiN(CF₃SO₂)₂, LiCF₃SO₃ and LiClO₄: Thermal properties and conductivity behavior. *Electrochim. Acta* **1992**, *37*, 1579–1583. [[CrossRef](#)]
10. Kim, G.T.; Appetecchi, G.B.; Carewska, M.; Joost, M.; Balducci, A.; Winter, M.; Passerini, S. UV cross-linked, lithium-conducting ternary polymer electrolytes containing ionic liquids. *J. Power Sources* **2010**, *195*, 6130–6137. [[CrossRef](#)]
11. Itoh, T.; Miyamura, Y.; Ichikawa, Y.; Uno, T.; Kubo, M.; Yamamoto, O. Composite polymer electrolytes of poly(ethylene oxide)/BaTiO₃/Li salt with hyperbranched polymer. *J. Power Sources* **2003**, *119–121*, 403–408. [[CrossRef](#)]
12. An, Y.; Cheng, X.; Zuo, P.; Liao, L.; Yin, G. Improved properties of polymer electrolyte by ionic liquid PP1.3TFSI for secondary lithium ion battery. *J. Solid State Electrochem.* **2012**, *16*, 383–389.
13. Jiang, Z.; Carroll, B.; Abraham, K.M. Studies of some poly(vinylidene fluoride) electrolytes. *Electrochim. Acta* **1997**, *42*, 2667–2677. [[CrossRef](#)]
14. Cao, J.H.; Zhu, B.K.; Xu, Y.Y. Structure and ionic conductivity of porous polymer electrolytes based on PVDF-HFP copolymer membranes. *J. Membr. Sci.* **2006**, *281*, 446–453. [[CrossRef](#)]
15. Liu, W.; Zhang, X.K.; Wu, F.; Xiang, Y. A study on PVDF-HFP gel polymer electrolyte for lithium-ion batteries. *IOP Conf. Ser. Mater. Sci. Eng.* **2017**, *213*, 012036. [[CrossRef](#)]
16. Herzog-Arbeitman, A.; Maletti, S.; Oswald, S.; Schmeida, T.; Giebel, L.; Mikhailova, D. A Highly Conductive Gel Polymer Electrolyte for Li-Mg Hybrid Batteries. *ACS Appl. Energy Mater.* **2021**, *4*, 1906–1914. [[CrossRef](#)]
17. Miao, R.; Liu, B.; Zhu, Z.; Liu, Y.; Li, J.; Wang, X.; Li, Q. PVDF-HFP-based porous polymer electrolyte membranes for lithium-ion batteries. *J. Power Sources* **2008**, *184*, 420–426. [[CrossRef](#)]
18. Croce, F.; Gerace, F.; Dautzenberg, G.; Passerini, S.; Appetecchi, G.B.; Scrosati, B. Synthesis and characterization of highly conducting gel electrolytes. *Electrochim. Acta* **1994**, *39*, 2187–2194. [[CrossRef](#)]

19. Bohnke, O.; Frand, G.; Rezrazi, M.; Rousselot, C.; Truche, C. Fast ion transport in new lithium electrolytes gelled with PMMA. 1. Influence of polymer concentration. *Solid State Ion.* **1993**, *66*, 97–104. [CrossRef]
20. Passerini, S.; Rosolen, J.M.; Scrosati, B. Plasticized carbon electrodes of interest for lithium rocking chair batteries. *J. Power Sources* **1993**, *45*, 333–341. [CrossRef]
21. Pistoia, G.; Antonini, A.; Wang, G. Impedance study on the reactivity of gel polymer electrolytes towards a lithium electrode. *J. Power Sources* **1996**, *58*, 139–144. [CrossRef]
22. Dias, F.B.; Plomp, L.; Veldhuis, J.B.J. Trends in polymer electrolytes for secondary lithium batteries. *J. Power Sources* **2000**, *88*, 169–191. [CrossRef]
23. Elamin, K.; Shojaatalhosseini, M.; Danyliv, O.; Martinelli, A.; Swenson, J. Conduction mechanism in polymeric membranes based on PEO or PVdF-HFP and containing a piperidinium ionic liquid. *Electrochim. Acta* **2019**, *299*, 979–986. [CrossRef]
24. Das, S.; Ghosh, A. Charge Carrier Relaxation in Different Plasticized PEO/PVDF-HFP Blend Solid Polymer Electrolytes. *J. Phys. Chem. B* **2017**, *121*, 5422–5432. [CrossRef] [PubMed]
25. Kim, K.M.; Park, N.G.; Ryu, K.S.; Chang, S.H. Characteristics of PVdF-HFP/TiO₂ composite membrane electrolytes prepared by phase inversion and conventional casting methods. *Electrochim. Acta* **2006**, *51*, 5636–5644. [CrossRef]
26. Xue, X.; Zhang, X.; Liu, Y.; Chen, S.; Chen, Y.; Lin, J.; Zhang, Y. Boosting the Performance of Solid-State Lithium Battery Based on Hybridizing Micron-Sized LATP in a PEO/PVDF-HFP Heterogeneous Polymer Matrix. *Energy Technol.* **2020**, *8*, 2000444. [CrossRef]
27. Shalu; Chaurasia, S.K.; Singh, R.K. Crystallization behaviour of a polymeric membrane based on the polymer PVdF-HFP and the ionic liquid BMIMBF₄. *RSC Adv.* **2014**, *4*, 50914–50924.
28. Zhang, P.; Li, R.; Huang, J.; Liu, B.; Zhou, M.; Wen, B.; Xia, Y.; Okada, S. Flexible poly(vinylidene fluoride- co - hexafluoropropylene)-based gel polymer electrolyte for high-performance lithium-ion batteries. *RSC Adv.* **2021**, *11*, 11943–11951. [CrossRef] [PubMed]
29. Manjunatha, H.; Damle, R.; Kumaraswamy, G.N. Modification of polymer electrolyte blend PEO/PVDF-HFP by low-energy O⁺ ion irradiation to improve electrolyte behavior. *Polym. Bull.* **2022**, *79*, 3929–3950. [CrossRef]
30. Ue, M.J. Mobility and Ionic Association of Lithium and Quaternary Ammonium Salts in Propylene Carbonate and γ-Butyrolactone. *Electrochim. Soc.* **1994**, *141*, 3336–3342. [CrossRef]
31. Kurzweil, P.; Dietlmeier, O.K. *Elektrochemische Speicher—Superkondensatoren, Batterien, Elektrolyse-Wasserstoff, Rechtliche Rahmenbedingungen*; Springer Vieweg: Wiesbaden, Germany, 2018.
32. Aurbach, D.; Talyosef, Y.; Markovsky, B.; Markevich, E.; Zinigrad, E.; Asraf, L.; Gnanaraj, J.S.; Kim, H.J. Design of electrolyte solutions for Li and Li-ion batteries: A review. *Electrochim. Acta* **2004**, *50*, 247–254. [CrossRef]
33. Heider, U.; Oesten, R.; Jungnitz, M. Challenge in manufacturing electrolyte solutions for lithium and lithium ion batteries quality control and minimizing contamination level. *J. Power Sources* **1999**, *81–82*, 119–122. [CrossRef]
34. Kawamura, T.; Okada, S.; Yamaki, J.I. Decomposition reaction of LiPF₆-based electrolytes for lithium ion cells. *J. Power Sources* **2006**, *156*, 547–554. [CrossRef]
35. Wiemers-Meyer, S.; Winter, M.; Nowak, S. Mechanistic insights into lithium ion battery electrolyte degradation-a quantitative NMR study. *Phys. Chem. Chem. Phys.* **2016**, *18*, 26595–26601. [CrossRef]
36. McEwen, B.; Ngo, H.L.; LeCompte, K.; Goldman, J.L. Electrochemical Properties of Imidazolium Salt Electrolytes for Electrochemical Capacitor Applications. *J. Electrochem. Soc.* **1999**, *146*, 1687–1695. [CrossRef]
37. Garcia, B.; Lavallée, S.; Perron, G.; Michot, C.; Armand, M. Room temperature molten salts as lithium battery electrolyte. *Electrochim. Acta* **2004**, *49*, 4583–4588. [CrossRef]
38. Bonhôte, P.; Dias, A.P.; Papageorgiou, N.; Kalyanasundaram, K.; Grätzel, M. Hydrophobic, Highly Conductive Ambient-Temperature Molten Salts. *Inorg. Chem.* **1996**, *35*, 1168–1178. [CrossRef]
39. Noda, A.; Hayamizu, K.; Watanabe, M. Pulsed-gradient spin-echo ¹H and ¹⁹F NMR ionic diffusion coefficient, viscosity, and ionic conductivity of non-chloroaluminate room-temperature ionic liquids. *J. Phys. Chem. B* **2001**, *105*, 4603–4610. [CrossRef]
40. Appetecchi, G.B.; Henderson, W.; Villano, P.; Berrettoni, M.; Passerini, S. PEO-LiN(SO₂CF₂CF₃)₂ Polymer Electrolytes: I. XRD, DSC, and Ionic Conductivity Characterization. *J. Electrochem. Soc.* **2001**, *148*, A1171–A1178. [CrossRef]
41. Meyer, W.H. Polymer Electrolytes for Lithium-Ion Batteries. *Adv. Mater.* **1998**, *10*, 439–448. [CrossRef]
42. Stephan, A.M. Review on gel polymer electrolytes for lithium batteries. *Eur. Polym. J.* **2006**, *42*, 21–42. [CrossRef]
43. Shalu; Singh, V.K.; Singh, R.K. Development of ion conducting polymer gel electrolyte membranes based on polymer PVdF-HFP, BMIMTFSI ionic liquid and the Li-salt with improved electrical, thermal and structural properties. *J. Mater. Chem. C Mater.* **2015**, *3*, 7305–7318. [CrossRef]
44. Diddens, D.; Heuer, A. Lithium ion transport mechanism in ternary polymer electrolyte-ionic liquid mixtures: A molecular dynamics simulation study. *ACS Macro Lett.* **2013**, *2*, 322–326. [CrossRef] [PubMed]
45. Pritam; Arya, A.; Sharma, A.L. Dielectric relaxations and transport properties parameter analysis of novel blended solid polymer electrolyte for sodium-ion rechargeable batteries. *J. Mater. Sci.* **2019**, *54*, 7131–7155. [CrossRef]

46. Prabakaran, P.; Manimuthu, R.P.; Gurusamy, S.; Sebasthiyan, E. Plasticized polymer electrolyte membranes based on PEO/PVdF-HFP for use as an effective electrolyte in lithium-ion batteries. *Chin. J. Polym. Sci.* **2017**, *35*, 407–421. [[CrossRef](#)]
47. Tian, X.; Jiang, X.; Zhu, B.; Xu, Y. Effect of the casting solvent on the crystal characteristics and pervaporative separation performances of P(VDF-co-HFP) membranes. *J. Memb. Sci.* **2006**, *279*, 479–486. [[CrossRef](#)]
48. An, Y.; Zuo, P.; Cheng, X.; Liao, L.; Yin, G. Preparation and properties of ionic-liquid mixed solutions as a safety electrolyte for lithium ion batteries. *Int. J. Electrochem. Sci.* **2011**, *6*, 2398–2410. [[CrossRef](#)]
49. Yu, B.; Zhou, F.; Wang, C.; Liu, W. A novel gel polymer electrolyte based on poly ionic liquid 1-ethyl 3-(2-methacryloyloxy ethyl) imidazolium iodide. *Eur. Polym. J.* **2007**, *43*, 2699–2707.
50. Choi, B. Optical microscopy study on the crystallization in PEO-salt polymer electrolytes. *Solid State Ion.* **2004**, *168*, 123–129. [[CrossRef](#)]
51. Bruce, P.G.; Vincent, C.A. Steady state current flow in solid binary electrolyte cells. *J. Electroanal. Chem. Interfacial Electrochem.* **1987**, *225*, 1–17. [[CrossRef](#)]
52. Evans, J.; Vincent, C.A.; Bruce, P.G. Electrochemical measurement of transference numbers in polymer electrolytes. *Polymer* **1987**, *28*, 2324–2328. [[CrossRef](#)]
53. Zhu, C.; Cheng, H.; Yang, Y. Electrochemical Characterization of Two Types of PEO-Based Polymer Electrolytes with Room-Temperature Ionic Liquids. *J. Electrochem. Soc.* **2008**, *155*, A569. [[CrossRef](#)]
54. Yamada, A.; Koizumi, H.; Nishimura, S.; Sonoyama, N.; Kanno, R.; Yonemura, M.; Nakamura, T.; Kobayashi, Y. Room-temperature miscibility gap in Li_xFePO_4 . *Nat. Mater.* **2006**, *5*, 357–360. [[CrossRef](#)] [[PubMed](#)]
55. Krause, L.J.; Lamanna, W.; Summerfield, J.; Engle, M.; Korba, G.; Loch, R.; Atanasoski, R. Corrosion of aluminum at high voltages in non-aqueous electrolytes containing perfluoroalkylsulfonyl imides; new lithium salts for lithium-ion cells. *J. Power Sources* **1997**, *68*, 320–325. [[CrossRef](#)]
56. Péter, L.; Arai, J. Anodic dissolution of aluminium in organic electrolytes containing perfluoroalkylsulfonyl imides. *J. Appl. Electrochem.* **1999**, *29*, 1053–1061. [[CrossRef](#)]
57. Scharner, S.; Weppner, W.; Schmid-Beurmann, P. Evidence of Two-Phase Formation upon Lithium Insertion into the $\text{Li}_{1.33}\text{Ti}_{1.67}\text{O}_4$ Spinel. *J. Electrochem. Soc.* **1999**, *146*, 857–861. [[CrossRef](#)]
58. Chawla, N.; Bharti, N.; Singh, S. Recent Advances in Non-Flammable Electrolytes for Safer Lithium-Ion Batteries. *Batteries* **2019**, *5*, 19. [[CrossRef](#)]
59. Polu, A.R.; Kareem, A.A.; Rasheed, H.K. Thermal, electrical and electrochemical properties of ionic liquid-doped poly(ethylene oxide)-LiTDI polymer electrolytes for Li-ion batteries. *J. Solid State Electrochem.* **2023**, *27*, 409–416. [[CrossRef](#)]
60. Chung, N.K.; Kwon, Y.D.; Kim, D. Thermal, mechanical, swelling, and electrochemical properties of poly(vinylidene fluoride)-co-hexafluoropropylene/poly(ethylene glycol) hybrid-type polymer electrolytes. *J. Power Sources* **2003**, *124*, 148–154. [[CrossRef](#)]
61. Kiefer, J.; Fries, J.; Leipertz, A. Experimental Vibrational Study of Imidazolium-Based Ionic Liquids: Raman and Infrared Spectra of 1-Ethyl-3-methylimidazolium Bis(Trifluoromethylsulfonyl)imide and 1-Ethyl-3-methylimidazolium Ethylsulfate. *Appl. Spectrosc.* **2007**, *61*, 1306–1311. [[CrossRef](#)]

Disclaimer/Publisher’s Note: The statements, opinions and data contained in all publications are solely those of the individual author(s) and contributor(s) and not of MDPI and/or the editor(s). MDPI and/or the editor(s) disclaim responsibility for any injury to people or property resulting from any ideas, methods, instructions or products referred to in the content.